Supercooling of liquid-metal droplets for x-ray-absorption-spectroscopy investigations

Luca Ottaviano and Adriano Filipponi
Dipartimento di Fisica, Università degli Studi dell' Aquila, Via Vetoio, 67010 Coppito, L'Aquila, Italy

Andrea Di Cicco
Dipartimento di Matematica e Fisica, Università degli Studi di Camerino, Via Madonna delle Carceri, 62032 Camerino, Italy

(Received 25 June 1993; revised manuscript received 17 December 1993)

A sample preparation technique, suitable for x-ray-absorption measurements of liquid and supercooled metals is described. The method is based on an application of the emulsion technique, consisting in a dispersion of micrometric droplets in an inert rigid matrix. It has been applied to Hg and Ga resulting in a very fine average droplet size in the submicrometer range. A theoretical probabilistic model, confirmed by experimental data, suggests a log-normal droplet-size distribution. The supercooling capabilities of the samples are studied by means of x-ray-absorption near-edge structure measurements showing exceptional supercooling rates: 153 K for Hg and no crystallization at all for Ga down to 34 K. The problem of a quantitative study of the x-ray-absorption fine structure is addressed and the nonlinearity in the absorption measurements induced by the nonuniform thickness distribution discussed. A method to calculate the sample metal thickness distribution and to derive the actual absorption coefficient is presented.

I. INTRODUCTION

In recent times attention has been paid to metastable states of condensed matter and in particular to supercooled and glassy metals.[1] In general, the metals that can be more easily supercooled are those whose crystallization occurs in low-symmetry phases and whose liquid local structure departs from the simple close packing. The supercooling capability of metals is often related to the appearance of polymorphism of the crystal phases in the P,T diagram. Supercooling in liquid metals has been studied initially from the morphologic and thermodynamic points of view. Earlier studies were carried out by Turnbull and Cech[2,3] by using samples of emulsified liquid-metal droplets. This technique was based on the observation that an efficient way to avoid crystal nucleation is to divide a metal specimen into a large number of isolated droplets. The main mechanism is the isolation of nucleation catalysts in a very small number of droplets. In the major part of the droplets nucleation takes place homogeneously and large rates of supercooling can be achieved. In the original works of Turnbull and Cech two main experimental observations were reported: (1) The crystal nucleation is retarded in isolated droplets of diameter less than 100 μm; (2) the smaller is the particle size, the lower is the solidification temperature. Maximum supercooling temperatures in the range 0.13–0.25 times the absolute melting temperature T_m were reported for various metal droplets. More recently, the droplet technique has been applied to various metals and compounds achieving very high rates of supercooling in the cases of gallium,[4] bismuth, and tin,[5] with typical droplets size of about 5–10 μm.

Study of supercooled states is particularly interesting from a microscopic point of view. In fact, little information is available about structural and electronic properties of supercooled liquids. A deeper insight into these problems can be provided by microscopic structural studies performed by means of x-ray and neutron-diffraction $[S(k)]$ or x-ray-absorption spectroscopies (XAS) $[\chi(k)]$. The supercooling phenomenon produces a freezing of the local disordered configurations that can be also used as a device to enhance the intensity of the structural signal and to improve the understanding of atomic correlations in liquids. Local structural information, generally limited to the pair distribution function (g_2), can be derived for supercooled liquids with the same procedures used for liquids in thermodynamical equilibrium.

Very recently, it has been pointed out that quantitative information about three-body correlations in disordered systems can be derived by XAS.[6] The sensitivity of the technique to higher-order distribution functions is due to the strong coupling between the local probe (excited photoelectron) and surrounding matter. The multiple-scattering signals contributing to the $\chi(k)$ probe the three-body (g_3), and the higher-order distribution functions and, at present, an appropriate method has been developed to extract structural information from experimental data.[6,7] The XAS structural information is intrinsically local because of the inelastic losses suffered by the photoelectron in the final state (mean free path $\lambda \approx 5$–10 Å). In addition, the large configurational disorder greatly reduces the intensity of the XAS experimental signal associated with higher-order distribution functions. For this reason very high signal-to-noise ratios are required. XAS provides complementary information to

those of x-ray and neutron diffraction, while additionally it represents a unique probe for the three-body distribution function. Clearly any information beyond the pair distribution function is useful for a better characterization of the average local liquid structure.

Due to various kinds of experimental difficulties, relatively few structural investigations on supercooled metals exist. X-ray-diffraction studies have been performed on supercooled Hg (Ref. 8 and Ga[9]). As far as x-ray-absorption measurements are concerned, although the importance of performing experiments on liquid systems can be easily acknowledged, a few studies have been realized so far.[10,11] The main technical problems are related to the preparation of the samples, which have to be homogeneous films of appropriate uniform thickness of pure substances. The appropriate thicknesses, depending on the particular edge considered, are typically 1–20 μm. XAS measurements on supercooled metals have been reported only for the Ga case.[12,13]

In this paper we present a method of preparation of samples which matches successfully the above-mentioned requirements for homogeneous thickness, together with the possibility of achieving exceptional rates of supercooling, by using the cited droplet technique. The samples were obtained using a dispersion of very small droplets in an inert, rigid, and x-ray transparent matrix. An accurate study of the droplet-size distribution is presented in order to justify the supercooling rates obtained in the experiment. This technique has been applied to the cases of liquid mercury and gallium. Possible future applications are limited to low melting point alloys. The supercooling properties of samples made dispersing micrometric particles and the treatment of the sample thickness unhomogeneities presented in this paper, are, however, widely general. The use of inert matrices stable at higher temperatures may allow further extensions of the technique.

The paper is organized as follows: In Sec. II the sample preparation method is described (Sec. II A), together with a theoretical probabilistic model and an accurate experimental study of the droplet-size distribution (Secs. II B and II C). The description of the XAS experiment, which demonstrates the supercooling capabilities for Hg and Ga, is reported in Sec. III. Finally, the problem of performing quantitative analysis and the correction of the effects related to the intrinsic metal thickness inhomogeneity of the sample are discussed in Sec. IV. Section V contains the conclusive remarks.

II. SAMPLE PREPARATION TECHNIQUE

A. Preparation method

The typical optimal metal thickness for absorption measurements is in the range 1–20 μm depending on the edge under investigation. In particular at the L_3 x-ray-absorption edge of Hg it is of the order of 6 μm, while at the K edge of Ga it is about 10 μm. A suitable way to gain such low thickness requirements, together with supercooling properties, is to produce slabs composed of a large number of micrometric droplets buried in an inert rigid matrix. In order to achieve very high supercooling rates the size of the droplets has to lie in the micrometer range, which is also a necessary condition to obtain a relatively uniform effective thickness for the metal component. A second requirement is that the rigid matrix absorption should be negligible, possibly yielding an absorptance smaller than 0.5 units.

In order to meet the previous requirements we used a two-component epoxy resin which guarantees a fast drying process and does not chemically react with mercury or gallium. A small quantity of metal (about 1% of the total glue volume) is mixed with one component of the glue, generating an emulsion by the mechanical pressure of a spatula (with a bladed edge) on a flat (typically glass) surface. Such procedure gradually breaks the droplets into ones of progressively smaller size. The mixing phase proceeds until the emulsion appears macroscopically homogeneous and the optical microscope inspection reveals micrometric dimensions for the droplets. Finally, the hardener component of the glue is added to the mixture and, before hardening, the fluid is poured into apposite slab-shaped shapes of suitable thicknesses. The final sample appears macroscopically as a thin uniform rigid slab. Microscopically, the emulsion is instead composed of a very large number of droplets of random diameter in the micrometer range. An accurate microscopic analysis of the emulsion can be performed on a very thin transparent layer deposited on a standard microscope slide (test slide). A microscope photograph of a typical Hg emulsion is shown as an example in Fig. 1. Notice the small Hg particles with dark circular shapes placed at random in the transparent glue matrix.

Because of the low-Z-element contents of the glue, it absorbs a negligible percentage of the x-ray beam and metal concentrations of the order of 1% in volume still produce samples in which the main absorber is the metal. With such a concentration the appropriate slab thickness becomes of the order of hundreds of micrometers.

The present technique can be extended to several low melting point alloys.

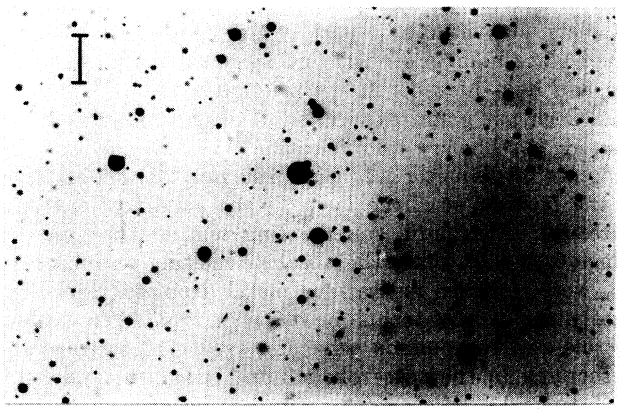

FIG. 1. Microscope photograph of the emulsion showing the mercury droplets; the bar corresponds to a 10 μm length.

B. Fragmentation probabilistic model

In order to interpret the experimental droplet distribution we developed a probabilistic model. Let us model the formation of the emulsion as the succession of discrete fragmentation steps of the metal droplets induced under the action of the spatula. After a single step j a generic droplet of mass m_0 may be either left unchanged or split into two or more, suppose n, droplets of masses $m_0 X_k^{(j)}, k \in (1,\ldots,n)$, where the $0 < X_k^{(j)} \leq 1$ are random variables, which obey the obvious mass conservation constraint $\sum_{k=1}^{n} X_k^{(j)} = 1$. After a large number of steps M the emulsion will contain many droplets. The mass of a single droplet can be described as the product of the original droplet mass m_0 times a large number of fragmentation variables,

$$m = m_0 X^{(1)} X^{(2)} X^{(3)} \cdots X^{(M)} , \qquad (1)$$

and therefore can be thought as the result of a random multiplicative process. Now, the final mass distribution will be determined by a very large number of sequences of this type. Actually, there is some correlation among the sequences which are generated by the same parent drop at a given step, but there will be still a lot of sequences which are uncorrelated in the last $L < M$ steps. We will also assume that the history of the particle does not affect the fragmentation probability and therefore that $\langle (X^{(j)} - \langle X^{(j)} \rangle)(X^{(k)} - \langle X^{(k)} \rangle) \rangle = 0$, for $j \neq k$. We will finally assume that the random variables $\ln(X^{(j)})$, defined in the interval $\ln(X^{(j)}) \leq 0$, have well defined moments with limited upper bounds.

The diameter of a droplet δ is proportional to the cubic root of its mass m; therefore, neglecting additive constants, the following relation holds for the experimental random variable λ defined as $\lambda \equiv \ln \delta$:

$$\lambda \sim \frac{1}{3}\ln(m) = \frac{1}{3}[\ln(m_0) + \ln(X^{(1)}) + \ln(X^{(2)}) + \ln(X^{(3)}) + \cdots + \ln(X^{(M)})] . \qquad (2)$$

Under the previous hypotheses, in the limit of a large number of steps $M \to \infty$, the central-limit theorem holds. Therefore the distribution of λ is predicted to approach a Gaussian distribution with a given mean $\langle \lambda \rangle = \bar{\lambda}$ and variance σ_λ^2. Consequently the droplet diameter distribution function $L(\delta)$ approaches a log-normal distribution, namely,

$$L(\delta) = \frac{1}{\delta\sqrt{2\pi\sigma_\lambda^2}}\, e^{-\frac{(\ln\delta - \bar{\lambda})^2}{2\sigma_\lambda^2}} . \qquad (3)$$

Some criticism to this log-normal model must be pointed out. In the real samples there are natural upper limits for the droplet size; these are, for instance, the diameter of the original droplet mixed with the glue and the slab thickness. Under the conditions in which we operated, these limits were well outside range of probable droplet radii, but even in this case they create problems when one tries to estimate the moments of the droplet diameter distribution from a sample. It is well known that the moments of the log-normal distribution grow much faster than $n!$ and therefore they are not well defined; the upper cutoff becomes progressively more important with increasing the order n of the moment. This inconsistency can be easily bypassed with (and justifies) the use of λ as the appropriate random variable to describe the droplet diameter distribution. λ is predicted to approach a Gaussian distribution whose parameters $\bar{\lambda}$ and σ_λ^2 can be easily estimated from a sample.

C. Droplet-size distribution (experimental determination)

As already mentioned, the supercooling capabilities of a liquid metal dispersed into droplets are intimately related to the average droplet size.[3] In order to exhaustively characterize the samples we performed a statistical analysis of the actual droplet-size distribution by means of an optical microscope analysis of the test slides. A series of photographs like the one reported in Fig. 1 were digitized and analyzed, with an appropriate software,[14] obtaining the diameters δ of a very large number of droplets. As an example of such an analysis we report in Fig. 2 the diameter probability density histograms $f(\delta)$ for three different samples. From top to bottom the histograms refer to a "coarse grain" Hg emulsion (a), a finely emulsified Hg sample used for the XAS measurements (b), and a Ga sample emulsion used in the experiment. Looking at Fig. 2 it is evident that in all cases the majority of the observed droplet diameters lies in the submicrome-

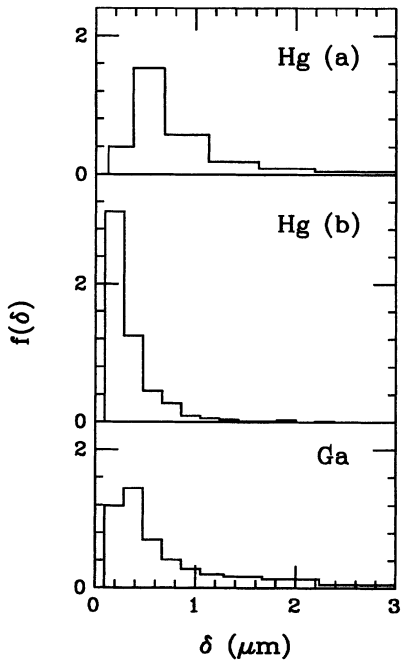

FIG. 2. From top to bottom: [Hg (a)] Histogram of the Hg droplets diameter of a coarse emulsion as determined from the microscope photographs analysis. δ is the droplet diameter in μm; in the ordinate scale the corresponding probability density $f(\delta)$ is reported; [Hg (b)] same for the Hg emulsion used for the XAS measurements; (Ga) same for the Ga sample.

ter range, indicating that the present emulsion preparation technique allows to achieve droplet sizes smaller than those previously reported in the literature for mercury[8] and gallium.[4] This is probably due to the great viscosity of the emulsifier, which prevents droplet reaggregation.

The droplet-size distribution presents an evident positive asymmetry with a significant number of large positive fluctuations in the diameters, confirming qualitatively what is expected from the log-normal model. This occurrence can be directly appreciated by a visual inspection of Fig. 1, noticing the occasional "giant" drops present in the emulsion. It should be noted that the optical microscope analysis does not allow any size distinction for particles smaller than 0.2–0.4 μm due to the obvious resolution limit given by the visible light wavelength. It is also likely that, due to contrast limitations, some smaller droplets are lost in the counts; for this reason the low diameter tail of the histograms should be taken with caution.

The statistical analysis in terms of the logarithmic variable λ is shown in Fig. 3. The order of the histograms corresponds to that of Fig. 2. The lack of information on the short distance tail of the histograms appears now to be widely expanded by the logarithmic scale. We performed a fit on the reliable part of the histograms minimizing the χ^2 residual between experimental data and theoretical Gaussian model. The fitting Gaussians are reported as solid lines in Fig. 3 that become dashed below the resolution limit of the analysis. The χ^2 test performed in the range of available experimental data confirms in the three cases the reliability of the log-normal model within the 90% confidence level. Clearly while the large diameter tail of the distribution can be accurately sampled the smaller diameter tail could be partially explored only for the Hg (a) and Ga samples. The number of measured droplets N and the fitting parameters $\bar{\lambda}$ and σ_λ^2 for the three droplet diameter distributions are reported in Table I. The present experimental findings are sufficient to support the log-normal model; in particular the predicted Gaussian shape is satisfactorily followed on the right lobe of the histograms. It should be noted that, as far as the XAS experiment is concerned, the probability to cross a single droplet, and therefore its weight in determining the sample absorption coefficient, is proportional to its cross section (diameter squared). Then the weight of a single droplet increases exponentially with $\ln(\delta) = \lambda$, that is, like $\exp(2\lambda)$. Thus possible ignorance on the left tail of the distribution affects in a negligible manner the final predicted spectrum.

In the next section the supercooling properties of these samples will be demonstrated.

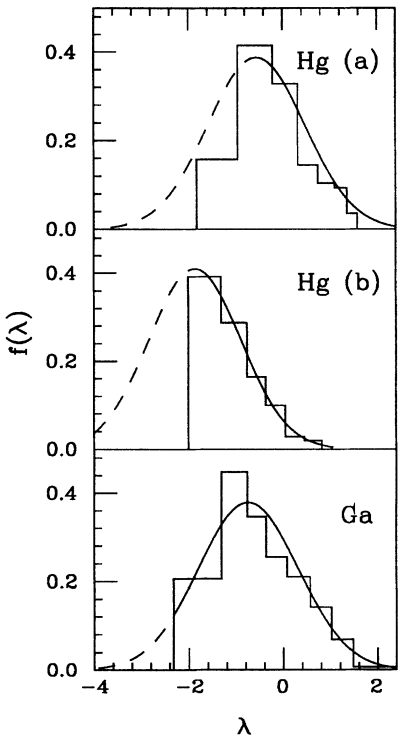

FIG. 3. Histograms of the logarithm of the Hg droplets diameter [Hg (a) and Hg (b)]. In the horizontal scale λ is the random variable $\ln(\delta)$ (δ is the droplet diameter in μm). The ordinate scale reports the corresponding probability density. The solid curves are the Gaussian fitting the histograms, with parameters $\bar{\lambda}$ and σ_λ^2, estimated from the sample; they are reported with dashed lines in the region below the corresponding optical microscope resolution limit. In the lower panel the corresponding histogram is reported for the Ga sample.

III. X-RAY-ABSORPTION MEASUREMENTS

X-ray-absorption measurements at the Hg L_3 edge (12 282 eV) and Ga K edge (10 367 eV) have been performed at the LURE laboratories (Orsay, Paris France) on the D42-EXAFS 1 beam line (bending magnet source) equipped with a Si (331) channel-cut monochromator during dedicated beam time. The ring was operating at 1.85 GeV with a typical current of 300 mA. The sample chamber was equipped with a He cryostat that allowed a fine temperature regulation.

The experiments have been performed by cycling the temperature going from above the melting points T_m of the metals to a low-temperature target. Fast x-ray-absorption near-edge-structure (XANES) spectra have been recorded lowering the temperature to monitor the increase of structural ordering, and in particular the occurrence of supercooling, the crystallization of the supercooled liquid, and the melting of the crystal above T_m. Spectra in a wider energy range have been also recorded for a quantitative study of the x-ray absorption fine structure (XAFS) subject to separate publications.[15,16]

TABLE I. Results of the statistical analysis of three emulsion samples; N is the number of counted droplets, and $\bar{\lambda}$ and σ_λ^2 are estimated average and variance of the logarithmic random variable λ.

Sample	N	$\bar{\lambda}$	σ_λ^2
Hg (a)	722	−0.55(8)	1.1(1)
Hg (b)	586	−1.9(1)	1.0(1)
Ga	823	−0.75(8)	1.1(1)

The XANES features are determined by the entire short-range atomic arrangement around the photoabsorber site. In this energy region the cross section is indeed affected by a full multiple-scattering regime where many higher-order distribution functions are involved. The current interpretation of the XANES is based on full multiple-scattering calculations, that allows one to obtain a qualitative identification of the local atomic distribution often resulting in information on the local symmetry or bond-angle values. In the specific case typical patterns for liquid and crystalline specimens can be easily recognized. Crystalline samples present characteristic sharper features, while, due to the large configurational disorder, the XANES of liquids is characterized by evident broader features.

A. Hg sample, evidence for supercooling

Several XANES spectra have been recorded at different temperatures in the energy range $E \in [12\,260, 12\,360]$ eV. Some representative spectra, recorded during the cooling and heating cycle, are reported in Fig. 4, and the corresponding derivatives with respect to the energy are reported in Fig. 5. The derivative curves allow a better identification of the differences among XANES spectra. Previous published spectra of liquid and polycrystalline Hg are in agreement with our data.[11] The cooling process has been carried out from room temperature down

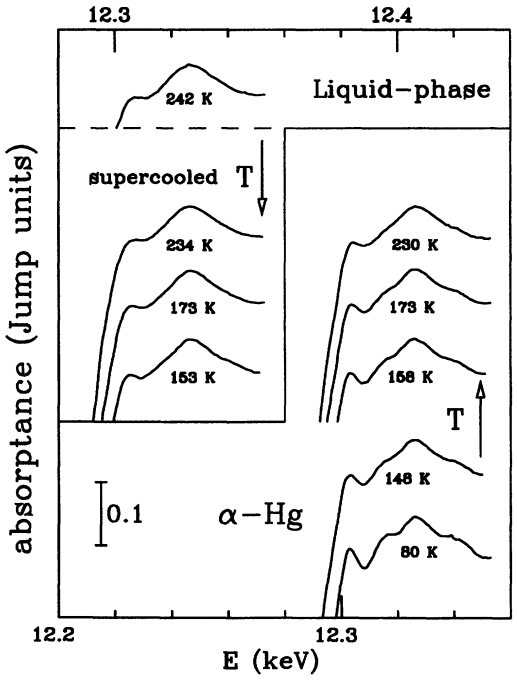

FIG. 4. Hg XANES spectra at various temperatures in the cooling and heating cycles. The upper and lower horizontal scales refer to the left-hand and right-hand curves respectively. The heights of all spectra are reported in terms of the absorptance main edge jump units (see the reference bar on the left-bottom side of the figure).

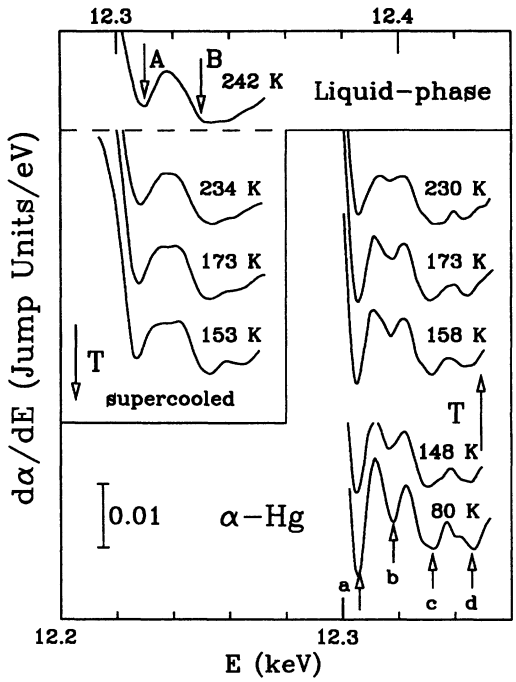

FIG. 5. Hg XANES derivative spectra. Each spectrum is labeled with the corresponding recording temperature. The upper and lower horizontal scales refer to the left-hand and right-hand curves respectively. The vertical scale spectra (see the reference bar on the left-bottom side of the figure) is in terms of (absorptance main edge jump units)/eV. The left curves belong to liquid and supercooled states, while the right ones refer to the sample crystallized in the α phase.

to 60 K with a rate of $\approx$ 60 K/h. Successively, the sample has been heated up to room temperature with the same rate. This procedure has been repeated several times providing similar results. During the typical XANES acquisition (lasting about 1 min) the temperature drift was less than 1 K.

The reference spectrum for the liquid phase, recorded at 242 K, 4 K above T_m=234.3 K, is reported in the upper sections of Fig. 4 and Fig. 5. The spectra, recorded during the cooling process, are reported in the middle-left sections, while spectra at nearly equivalent temperatures recorded during the heating process are shown in the middle-right sections. No abrupt change of the XANES spectra during the cooling process is seen at T_m while such an effect has been observed at about 150 K, indicating a retarded crystallization of the droplets. Below this temperature the spectra recorded during the cooling and heating processes were indistinguishable (lower panels), while an evident hysteresis is shown in the temperature range (150 K $-$ T_m) by the middle-right section spectra, indicating the presence of nonequilibrium supercooled states.

The XANES reported in the lower panels are representative of the α-Hg crystalline phase.[17] The α phase is stable at ordinary pressures certainly above 90 K.[18,19] At lower temperatures α-Hg is metastable, but the application of an external pressure of at least a few tenths of GPa is required to induce a transition to the stable phase

β-Hg (Ref. 19). Hg droplets cooled down to 5 K were observed to crystallize and maintain the α-Hg structure[17]. The crystallization of Hg droplets into the β-Hg phase, or even in the other high-pressure structures γ and δ,[20] has never been observed and is anyway unlikely. In addition, an analysis of the extended XAFS (EXAFS) oscillations (not included in this paper) indicates undoubtedly that our sample crystallized in the α-Hg phase.

The α-Hg spectra present sharp features and, in particular, one can identify four successive minima (a, b, c, and d) in the derivative spectrum (Fig. 5). These features are extremely sharp in the 80 K spectrum due to the freezing of thermal vibrations, but, despite a smearing due to increased Debye-Waller effects, they can be also easily identified in the other spectra, reported in the middle-right panels, up to T_m. We verified that raising the temperature above T_m a sudden change of the spectra occurs, for the crystallized samples, corresponding to the melting in thermodynamic equilibrium conditions.

In spite of the very fine droplet distribution the XAS signal is dominated by the contribution of droplets in the μm range, which, as far as the melting point is concerned, behave like bulk Hg.[3]

Differently from the crystalline one, the liquid Hg derivative XANES shows only two broader minima (A and B) which are also detectable in the supercooled spectra (middle-left sections). Lowering the temperature in the supercooled state, minima A and B become progressively sharper and, in particular, the B minimum appears to split into two minima, apparently similar to c and d. However, this splitting is not accompanied by a simultaneous appearance of the sharp features a and b of the solid. Thus minima c and d must be associated with an increase of local ordering, independent of the appearance of the long-range order typical of crystalline phases. We estimated that in the 153 K supercooled sample there is no evidence for the presence of a macroscopic percentage of crystallized droplets exceeding about 5%. The abrupt change of the spectra during the cooling process observed at about 150 K indicates a simultaneous crystallization of all the droplets within a 5 K range.

The present investigation demonstrates the supercooling capabilities of the Hg emulsion in epoxy resin with micrometric droplet sizes, reaching the limiting supercooling temperature of 153 K [relative supercooling ratio $(T_m\text{-}T_{sc})/T_m \approx 0.36$] which is slightly lower than previous rates: 173 K reached by Bosio.[8]

B. Ga sample

Gallium K-edge XANES spectra of the above-mentioned emulsions of micrometric droplets (hereafter called sample S) have been recorded at different temperatures in the energy range $E \in [10\,330, 10\,430]$ eV. Cooling-heating cycles were performed similarly to the Hg case with lower limiting temperature of 34 K. Fast XANES acquisitions, performed during the cooling (heating) processes, allowed us to monitor the continuous ordering (disordering) of local structure. Low-noise spectra which required longer acquisition time were recorded at the temperatures of 310 K, 298 K, 200 K, 124 K, 80 K, and 34 K. X-ray-absorption spectra at 310 K, representative of liquid gallium in thermodynamic equilibrium, have been recorded several times on different specimens. XANES spectra of a reference sample (hereafter called sample C) of solid crystalline gallium, prepared as a thin film (about 10 μm thick) of pure gallium (Ventron-Alfa 99.99%) held within two Kapton sheets, have been measured at 295 K and, below the melting point (T_m=302.9 K), at the same temperatures of the S sample. Spectra recorded at five different temperatures of both specimens S and C are reported in Fig. 6, in the lower-left and lower-right panels respectively. A XANES spectrum of liquid gallium is reported in the upper panel of Fig. 6 for comparison. It is evident that XANES spectra of the two samples are different throughout the overall thermal cycle. Both spectra preserve the same shape in the entire range of temperatures investigated, without showing any hysteresis effect, indicating that local structure is not subject to abrupt changes, contrary to the Hg case. This has to be expected for the crystalline sample C, representative of crystalline gallium (right panel), as temperature has been maintained below the melting point. In the case of the sample S, the XANES spectra show exactly the same features characteristic of the liquid phase. The absence of signatures of phase transitions means that crystallization has not taken place and indicates the presence of large rates of supercooling. The lack

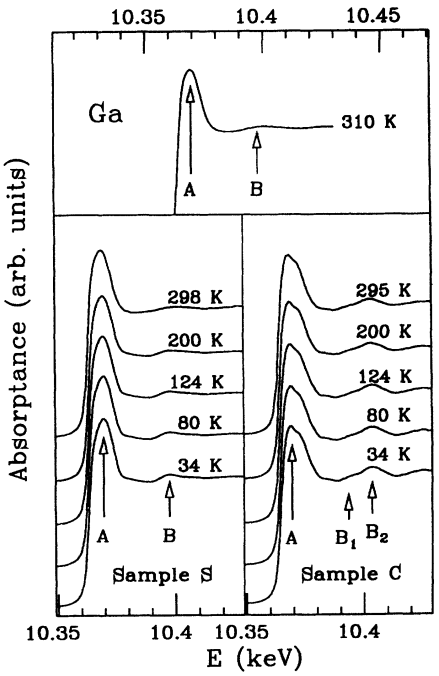

FIG. 6. Ga XANES spectra. Each spectrum is labeled with the corresponding recording temperature. The lower-left panel spectra were obtained with a Ga/epoxy resin emulsion (sample S); the lower-right panel spectra refer to a 10 μm uniform Ga layer sample in the crystalline phase (sample C). The upper panel reports the liquid-phase reference spectrum.

of abrupt changes has been verified by repeating many times the thermal cycles (below and above the melting point) and observing the continuous slight sharpening or broadening of the XANES features obtained decreasing or increasing the temperature. In particular, one can verify that the white line A preserves the same rounded shape in liquid gallium and in the spectra of sample S of the lower-left panel. On the contrary, the white line of crystalline gallium has throughout a different shape with a shoulder in the right side. Moreover, one can identify a second feature B in the XANES of liquid gallium, which gradually shifts a few eV and becomes more evident in sample S with decreasing the temperature. On the other hand, spectra of crystalline gallium are characterized by two peaks B_1 and B_2 which are not detectable either in the liquid or in the supercooled sample. From these observations we conclude that the preparation procedure described in this paper allows one to produce a specimen of gallium that does not crystallize down to 34 K. Crystallization to other crystalline phases, different from α-Ga, is also ruled out by the absence of sudden changes of XANES spectra. Moreover, the presence of a high level of structural disorder of the atomic structure of the S sample is also confirmed by EXAFS analysis.[16] Of course, at very low temperature, viscosity is so high that atomic diffusion is not possible anymore. A theoretical estimate for a glass transition temperature of 74 K, in the case of gallium,[21] suggests that below this temperature atomic configurations are frozen in a metastable state characterized by static disorder. In conclusion we demonstrated that Ga emulsions of the type presented in this paper allow one to reach exceptional supercooling rates (up to the theoretical limit) in a continuous and reversible way, overcoming previously established experimental limits of 200 K (Ref. 4) and 180 K,[12] corresponding to relative supercooling ratios $(T_m\text{-}T_{sc})/T_m$ in the range 0.33–0.40.

IV. THICKNESS INHOMOGENEITIES

A. Effects on the signal

In order to perform a quantitative structural analysis of the XAS signal the measurement should provide a quantity proportional to the absorption cross section, which generally requires a sample of constant thickness. It is clear that the samples prepared with the emulsion technique, as far as the x-ray-absorption measurements are concerned, have an effective metal thickness that varies randomly point to point over the surface of the sample orthogonal to the x-ray beam, the thickness depending roughly on the number and size of crossed droplets. Clearly in the limit of very small droplet sizes (and consequently a large number of droplets intercepted by each ray) the thickness tends to be uniform. Conversely if the average dimension of the droplets is (>1 μm) comparable to the total effective metal thickness ($\approx$ 6 μm for Hg) the thickness variation are not negligible anymore.

The effects on the absorption measurements in the case of samples of variable thickness have been widely discussed in literature.[22,23] Nevertheless in the present context we shall develop a specific treatment and derive a few useful equations. Let us consider the sample thickness $l = l(x,y)$ as a random variable defined on the plane orthogonal to the beam direction. If I_0 and I_1 are the incident and transmitted intensities respectively, assuming a constant flux in the beam section, then the intensity I_1 revealed after the sample will be

$$I_1 = \frac{1}{S}\int_S dxdy \quad I_0 e^{-\mu l(x,y)} = I_0 \int_0^\infty dl \quad P(l)e^{-\mu l} \ , \quad (4)$$

where μ is the absorption coefficient per unit length at a given energy. In the right-hand side integral we have introduced the thickness probability density $P(l)$. The expression is proportional to the moments generatrix function of the random variable l: $G_l(t) \equiv E\{\exp(tl)\}$ calculated at the value $t = -\mu$ of the parameter t. $E\{\cdots\}$ stands for *expected value of* . As usual the absorptance is defined as

$$\alpha = \ln \frac{I_0}{I_1} = -\ln G_l(-\mu) \equiv -\Phi_l(-\mu) \ , \quad (5)$$

where by definition $\Phi_l(t)$ is the cumulant generatrix function of the random variable l. $\Phi_l(t)$ can be expanded in powers of t according to the well known cumulant expansion

$$\Phi_l(t) = \sum_{j=1}^{\infty} \frac{K_j}{j!} t^j \ , \quad (6)$$

where K_j are the cumulants of the distribution. The first four cumulants expressed in terms of the moments about the mean $M_n(\bar{l})$ are given by

$$\begin{aligned} K_1 &= \bar{l}, \\ K_2 &= M_2(\bar{l}) \equiv \sigma_l^2, \\ K_3 &= M_3(\bar{l}), \\ K_4 &= M_4(\bar{l}) - 3M_2(\bar{l})^2. \end{aligned} \quad (7)$$

According to Eqs. (5) and (6) the experimental absorptance results

$$\ln \frac{I_0}{I_1} = K_1\mu - \frac{K_2}{2}\mu^2 + \frac{K_3}{3!}\mu^3 - \frac{K_4}{4!}\mu^4 + \cdots . \quad (8)$$

From Eq. (8) it is evident that the absorptance coincides with $\mu\bar{l}$ only in the case of a singular thickness distribution $P(l) = \delta(l - \bar{l})$, while, in general, nonlinear corrections appear. For instance, considering a sample with a Gaussian thickness distribution with variance σ_l^2 the observed absorptance would be

$$\ln \frac{I_0}{I_1} = \mu\bar{l} - \frac{\sigma_l^2}{2}\mu^2 \ . \quad (9)$$

Equation (9) contains a nonlinear correction that underestimates the absorption coefficient especially in correspondence of its maxima. In general a sample inho-

mogeneity produces a flattening of the x-ray-absorption spectrum, which increases as the moments of the thickness distribution become larger. The nonlinearity of Eq. (8) is in general an intrinsic problem in powder or droplets samples, but as we shall see, the accurate knowledge of the moments of the thickness distribution allows one to estimate and eventually remove the nonlinear corrections.

B. Sample thickness distribution

The thickness distribution function and relative corrections can be estimated in several simple cases of inhomogeneities. For instance a sample of thickness l_0 with a hole affecting a percentage a of the sample surface produces a $P(l) = a\delta(l) + (1-a)\delta(l-l_0)$, and a wedged shape sample produces a uniform thickness distribution in a given thickness range. From these models the cumulants, or even the whole generatrix function, can be directly calculated.

For the emulsified samples presented in this work the reliable probabilistic model for the droplet diameter previously formulated can be used to derive the actual sample thickness distribution by using a computer simulation. In the following we shall consider the Hg case for which the thickness requirements are more stringent. For such simulation we used the accurate experimental information on the droplets-size distribution (Table I) together with the above mentioned log-normal model (Sec. II B) for a droplet fragmentation. Spheres with random diameters (with a log-normal distribution with parameters $\bar{\lambda}$ and σ_λ^2; see Table I) were positioned at random into a slab volume of realistic thickness. Excluded volume problems were considered by eliminating all new spheres overlapping those previously positioned. The droplet density was given according to the measured metal concentrations (1.3% into the true Hg sample). The presence of an upper bound for the droplet radii was also considered.

For any ray striking onto the sample it is straightforward to calculate the local effective metal thickness. The sample metal thickness distribution has been obtained sampling a very large number of parallel rays placed at random on the simulated slab. The corresponding histogram for the Hg case is shown in Fig. 7 which represents the simulated probability density $P(l)$. The simulation allowed also a reliable evaluation of the cumulants up to the fourth order.

By means of this kind of simulation one can discriminate whether the nonlinear corrections of the absorption signal are important or not. In the case of an average drop diameter smaller than 1/20 of the optimal thickness of the sample, the sample can be considered uniform in thickness. In our case the distribution is broad enough to generate nonlinear corrections in the absorptance of the order of the 15% which should be taken into account.

C. Data correction

The target of any XAS experiment is to measure the actual absorption coefficient μ (proportional to the cross

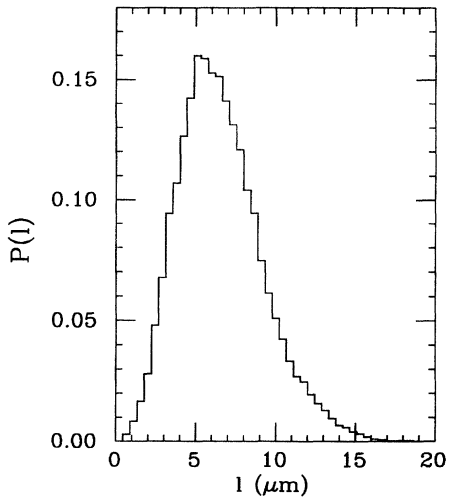

FIG. 7. Histogram of the thickness distribution in the simulated Hg sample. The abscissa l is the random sample thickness; the ordinate scale reports the corresponding probability density $P(l)$.

section). This aim can be achieved either by using samples with negligible thickness fluctuations or, provided the thickness distribution and its cumulants are known, solving for μ Eq. (8). This can be obtained using an iterative procedure based on the equation

$$\bar{l}\mu = \alpha + \frac{K_2}{2}\mu^2 - \frac{K_3}{3!}\mu^3 + \frac{K_4}{4!}\mu^4 - \cdots \qquad (10)$$

starting from $\mu = 0$. Notice that the nonlinear corrections are of the order of $K_j/(j!\,(\bar{l})^j)$ and are usually small enough to guarantee a fast convergence of the iteration.

Let us now consider a specific example of the procedure for correcting the raw data from the nonlinear corrections due to the inhomogeneities of the thickness. In Fig. 8 we report the experimental Hg L_3 299 K spectrum as measured (labeled $\alpha_{\rm exp}$) and the same spectrum after the application of the nonlinear corrections performed according to Eq. (10) with the cumulants derived from the computer simulation (labeled $\alpha_{\rm corr}$). The corrected spectrum is about 15% higher than the measured one, but the amplification factor is not constant, the peaks of the spectrum being subject to a larger magnification. Anyway, the nonlinear effects are only of the order of a few percent as shown at the bottom of the figure by the ratio $(\alpha_{\rm exp}/\alpha_{\rm corr})$ between the two spectra. Moreover the differences between the relative extracted fine structure signals are indeed negligible (being, at maximum, of the order of 0.002 of the absorptance jump value) as shown in Fig. 9.

This example shows that, although our preparation technique provides samples intrinsically affected by thickness inhomogeneities, this problem can be successfully taken under control. Besides, the droplet-size analysis, in conjunction with a computer simulation, allows one to calculate reliably the first cumulants of the thickness distribution and to apply the nonlinear corrections accounting for the main systematic errors affecting the data.

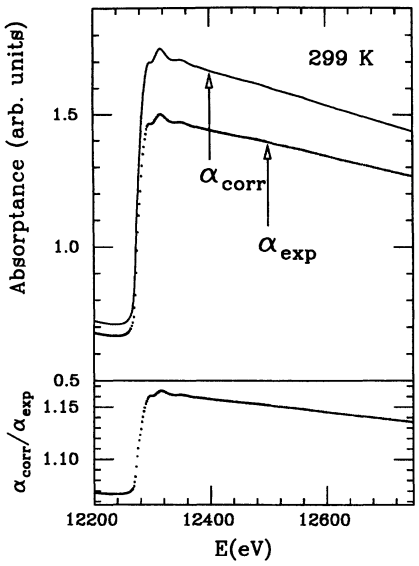

FIG. 8. Raw absorption spectrum of liquid Hg at 299 K (α_{exp}, dotted curve), the same spectrum corrected for the nonlinear terms (α_{corr}, solid curve), and (lower panel) ratio ($\alpha_{exp}/\alpha_{corr}$) between the two spectra. The horizontal scale reports the x-ray photon energy in eV.

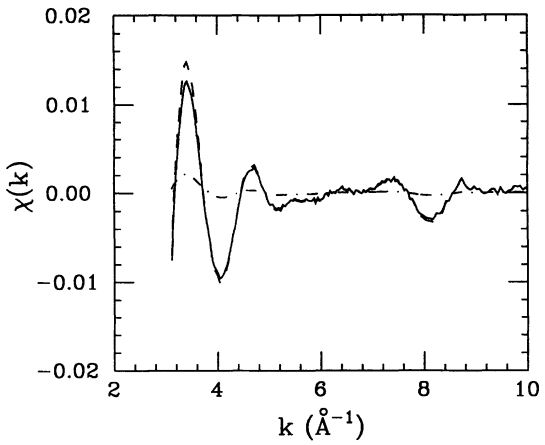

FIG. 9. EXAFS spectra of liquid Hg at 299 K before and after the nonlinear correction for the sample inhomogeneity, solid and dashed curves respectively. The dot-dashed curve is the difference between the dashed and solid curve. The horizontal scale reports the photo electron wave vector k in Å^{-1}; the ordinate scale reports dimensionless units representing the ratio between the structural oscillations of the absorption coefficient and the corresponding atomic background. The nonlinear corrections are therefore lesser than 0.002. In the background no account was taken for the $2p_{3/2}4f$ double-electron excitation edge at $k \approx 6$ Å^{-1}.[24]

V. CONCLUSIONS

In the present work we described a novel sample preparation technique, suitable for x-ray-absorption measurements of liquid and supercooled metals. The samples are emulsions of micrometric metal droplets in an inert rigid matrix. At present the method proved to be useful to confine liquid samples with micrometric thickness in the case of metals with very large surface tension like Hg.

The technique has been applied to Hg and Ga where a microscope analysis of the emulsions revealed a very fine average droplet size in the submicrometer range. We developed a probabilistic model which provides a theoretical prediction (log-normal) for the droplet-size distribution. This model was directly verified by comparing it with experimental droplets distributions. By using the sample preparation technique we recently succeeded to perform an accurate XAS experiment on liquid Hg (Ref. 15) and Ga.[16] Possible future applications will concern extensive investigations of supercooled liquids by XAS, which would provide complementary information with respect to $S(k)$ measurements.

The supercooling capabilities of the samples have been studied by XANES spectra as a function of the sample temperature obtaining exceptional supercooling rates: 153 K for Hg and no crystallization at all for Ga down to 34 K. Clearly the quantitative structural analysis should be possibly performed on XAS spectra taken in a wider energy range including many EXAFS oscillations.

The intrinsic inhomogeneous nature on the samples provides absorption spectra distorted by nonlinear effects. In order to obtain accurate x-ray-absorption structural data we developed a method to calculate the actual sample metal thickness distribution and to derive the actual absorption coefficient. The XAS investigations on liquid and supercooled metal that are now being undertaken will benefit from the extensive application of these procedures.

ACKNOWLEDGMENTS

Thanks are due to Dr. G. Chichiriccò (Dipartimento di Scienze Ambientali of the Università dell'Aquila) for microscope photographic work, and to Dr. Maria Giammatteo (Centro di Microscopia Elettronica, Università dell'Aquila) for the digital analysis of the pictures. The skillful operation of DCI storage ring by the LURE staff is particularly acknowledged, as well as the local support by Professor A. Sadoc and Professor P. Lagarde. We are also greatly indebted to F. Villain of the LURE technical staff.

[1] M.I. Klinger, Phys. Rep. **165**, 275 (1988); J. Jäckle, Rep. Prog. Phys. **49**, 171 (1986).
[2] D. Turnbull and R. E. Cech, J. Appl. Phys. **21**, 804 (1950); D. Turnbull, J. Appl. Phys. **21**, 1022 (1950).
[3] D. Turnbull, J. Chem. Phys. **20**, 411 (1952).
[4] Y. Miyazawa and G. M. Pound, J. Cryst. Growth **23**, 45 (1974).
[5] D. H. Rasmussen and C. R. Loper, Jr., Acta Metall. **23**, 1215 (1975).
[6] A. Filipponi, A. Di Cicco, M. Benfatto, and C. R. Natoli, Europhys. Lett. **13**, 319 (1990).
[7] A. Filipponi, A. Di Cicco, T. A. Tyson, and C. R. Natoli,

Solid State Commun. **78**, 265 (1991).
[8] L. Bosio, R. Cortes, and C. Segaud, J. Chem. Phys. **71**, 3595 (1979).
[9] A. Bererhi, A. Bizid, L. Bosio, R. Cortes, A. Defrain, and C. Segaud, J. Phys. (Paris) Colloq. **41**, C 8-218 (1980).
[10] E. D. Crozier and A. J. Seary, Can. J. Phys. **58**, 1388 (1980); B. R. Orton, G. K. Malra, and A. T. Steel, J. Phys. F **17**, L45 (1987); E. A. Stern, P. Līviņš, and Z. Zhang, Phys. Rev. B **43**, 8850 (1991).
[11] E. D. Crozier, in *EXAFS Spectroscopy: Techniques and Applications*, edited by B. K. Teo and D. C. Joy (Plenum, New York, 1981).
[12] J. P. Badiali, L. Bosio, R. Cortes, P. Bondot, G. Loupias, and J. Petiau, J. Phys. (Paris) Colloq. **41**, C8-211 (1980).
[13] M. Hida, H. Maeda, N. Kamijo, K. Tanabe, H. Tearuchi, Y. Tsu, and S. Watanabe, J. Non-Cryst. Solids **61-62**, 415 (1984).
[14] Courtesy of Dr. Maria Giammatteo, Centro di Microscopia Elettronica, Facoltà di Ingegneria, L' Aquila.
[15] L. Ottaviano, A. Filipponi, A. Di Cicco, S. Santucci, and P. Picozzi, J. Non-Cryst. Solids **156-158**, 112 (1993).
[16] A. Di Cicco and A. Filipponi, J. Non-Cryst. Solids **156-158**, 102 (1993).
[17] C.S. Barrett, Acta Crystallogr. **10**, 58 (1957).
[18] C. A. Swenson, Phys. Rev. **111**, 82 (1958).
[19] M. Atoji, J. E. Schirber, and C. Swenson, J. Chem. Phys. **31**, 1628 (1959).
[20] O. Schulte and W. Holzapfel, Phys. Rev. B **48**, 14 009 (1993).
[21] J. Watcher and F. Sommer, J. Non-Cryst. Solids **117-118**, 890 (1990).
[22] J. Goulon, C. Goulon Ginet, R. Cortes, and M. Dubois, J. Phys. (Paris) **43**, 539 (1982).
[23] E. A. Stern and K. Kim, Phys. Rev. B **23**, 3781 (1981).
[24] A. Filipponi, L. Ottaviano, and T. A. Tyson, Phys. Rev. A **48**, 2098 (1993).

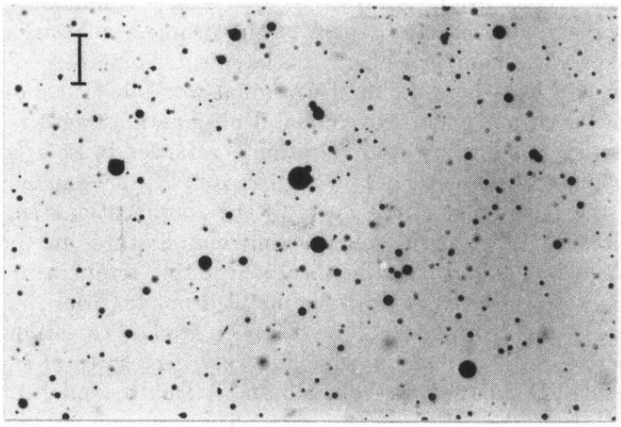

FIG. 1. Microscope photograph of the emulsion showing the mercury droplets; the bar corresponds to a 10 μm length.